ACS OMEGA

Open Access

This article is licensed under CC-BY-NC-ND 4.0

http://pubs.acs.org/journal/acsodf

Article

Quantitative Characterization of Adhesion Work on Shale Surfaces and Discussion on the Influence of Roughness Based on Atomic Force Microscopy (AFM)

Xu Huo, Linghui Sun,* Feiyu Chen, Zhengming Yang, Xiuxiu Pan, Junqian Li, Zhaojing Song, Zhirong Zhang, and Chun Feng

Cite This: *ACS Omega* 2024, 9, 30859−30872

Read Online

ACCESS | Metrics & More | Article Recommendations

ABSTRACT: Adhesion is an intrinsic property of rocks and liquids. Investigating the factors contributing to its formation and the mechanisms governing its action is crucial for elucidating the adhesion work between solids and liquids. The adhesion work, serving as a parameter that characterizes the energy changes during the solid−liquid contact process, is a vital tool for probing this phenomenon. However, conventional measurements of the adhesion work are significantly influenced by surface roughness and fail to differentiate local variations in the adhesion performance. This limitation obscures our understanding of the primary adsorption sites and mechanisms between solids and liquids, posing significant challenges to the study of rock surface properties. In this study, in conjunction with scanning electron microscopy and contact angle analyses, we elucidated for the first time the locations where voids form during the solid−liquid contact process, the lithological composition of rough areas, and their impact on the adhesion work between water/oil and the surfaces. Additionally, employing atomic force microscopy (AFM), we examined the variations in water/oil−solid adhesion work across different characteristic regions, thereby characterizing the overall hydrophilic/hydrophobic properties of the rock core. Specific conclusions are as follows: (1) A negative correlation exists between roughness and the contact angle adhesion work, with heterogeneity impeding liquid-rock contact; (2) By comparing the strength of water−solid/oil−solid adhesion work within localized areas, we delineated the adhesion work characteristics of samples and their primary generation sites, with oil−solid adhesion work in target blocks predominantly originating from quartz, clay minerals, and organic matter; (3) The influence of pore throat development on the overall adhesion work of samples was clarified, demonstrating that an increase in the proportion of internal rock pores enhances the surface oil−solid adhesion work; (4) A dimensionless wetting index *I* was established to mitigate the impact of roughness on the expression of adhesion work, exhibiting a strong correlation with traditional evaluation methods.

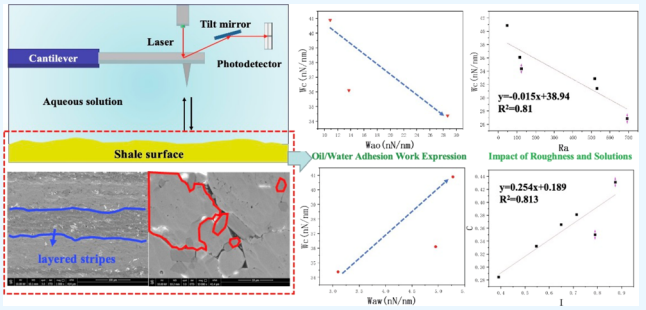

1. INTRODUCTION

Globally, the increasing demand for petroleum resources and the depletion of conventional oil and gas reserves have led to significant attention for unconventional reservoirs. Among these, shale formations have garnered immense interest, with global technically recoverable resources reaching up to 700−800 billion tons, prompting extensive exploration.[1−3] However, this heightened interest is accompanied by significant challenges.[4,5] Regarding solid−liquid interactions, the heterogeneity of reservoir pore structures, variations in lithological segments, and mineral components can cause fluctuations in the adhesion work to crude oil, contributing to the complexity of mixed wetting distributions,[6−8] thereby rendering macroscopic evaluation methods insufficient for accurately characterizing microscopic adhesion phenomena.[9] Thus, accurately assessing solid−liquid interactions at the microscopic level in shale formations, identifying the primary adsorption sites of crude oil, and exploring related influencing factors are crucial for understanding crude oil storage spaces and enhancing oil detachment efficiency.

In the petroleum industry, the investigation of solid−liquid adhesion capacity under varying conditions has remained a focal point.[10−12] Essentially, owing to intermolecular forces,[13,14] the distance between solid and liquid phases

Received: April 16, 2024
Revised: June 13, 2024
Accepted: June 21, 2024
Published: July 3, 2024

© 2024 The Authors. Published by American Chemical Society

progressively decreases until they come into close proximity.[15,16] This mutual attractive force is primarily represented by the adhesion work, a pivotal indicator for evaluating energy changes between solid and liquid phases.[11,15,16] Upon alterations in external or sample physical conditions, the adhesion work either strengthens or weakens, influenced by factors such as surface roughness, temperature, mineral composition, and surface organic matter adsorption.[6,7,17−21] Under constant external conditions, mineral distribution, organic matter adsorption, and surface roughness are regarded as the principal factors influencing solid−liquid adhesion.

On the one hand, scholars have delved into the particularity of rock surface wettability from a physical perspective. It has been reported that surfaces of minerals like quartz, feldspar, and clay exhibit hydrophilicity,[22−24] while carbonate rock minerals tend to be more hydrophobic.[17,25−27] This distinction primarily arises from the surface properties of the minerals. Due to variations in adhesion work between water-rock and oil-rock, samples exhibit varying degrees of adsorption capacity when in contact with crude oil. However, this conclusion is valid only under clean conditions; in the presence of organic matter in reservoir spaces, internal hydrophobic polycyclic aromatic hydrocarbons undergo spontaneous coupling with hydrophilic polar groups, adsorbing onto solid surfaces.[28,29] This process alters the wetting equilibrium among solid/liquid/gas phases by modifying the distribution of charged particles on the solid surface and interfacial tension, thereby influencing the adhesion between rock and liquid. (Note that interfacial tension is closely associated with the expression of surface adhesion work. Changes in the distribution of surface charges directly affect the surface energies of solids. When surface charges are more densely distributed, the surface energy also increases. Surface energy is directly related to surface tension and exhibits a positive correlation. Therefore, the distribution and density of surface charges will directly impact surface tension, consequently affecting wettability). Studies have shown that adsorbed asphaltene on solid surfaces can alter surface wettability.[28−32] Consequently, the resulting mixed wetting distribution varies due to different oil film binding sites in local spaces.[8,9]

On the other hand, the influence of roughness lies in the evaluation process of adhesion.[33] According to the Wenzel and Cassie models,[34,35] when rocks are relatively hydrophobic, increasing surface roughness can significantly increase the contact angle of water droplets. Although surface roughness can be controlled through grinding and polishing to some extent, it only addresses the large scratches produced during cutting processes,[36] failing to completely resolve the heterogeneous nature of rocks caused by brittle fractures and depressions between small-sized mineral grains. For traditional contact angle methods, air entering rough areas hinders solid−liquid contact, resulting in measurement inaccuracies that do not fully reflect the adhesion work of samples.[34,35] Additionally, traditional methods struggle to effectively characterize the contribution of local adhesion and to evaluate and distinguish the main development positions of oil−solid/water−solid adhesion work, leading to an unclear understanding of the main oil-wet/water-wet spaces of the samples. This affects the accuracy of crude oil storage evaluations and the oil film detachment efficiency. Thus, directly measuring the distribution of oil-rock adhesion work at the microscopic level is crucial for clarifying residual oil adhesion states, microscopic oil binding mechanisms, and their controlling factors, addressing issues such as low oil detachment efficiency.

In recent years, the application of atomic force microscopy (AFM) in nanoscale research has increased.[37,38] Initially, AFM's nanoscale tip was primarily used for scanning rock surfaces, generating two-dimensional (2D) and three-dimensional (3D) topographic maps.[39] With the maturity of force−indentation mode, AFM can provide mechanical information about scanned material stiffness and sample orientation toward the tip.[37,39] Some researchers have modified gold-coated AFM probes for studying the interaction mechanisms between specific functional groups and solids, elucidating the predominant mechanical actions experimentally.[40−42] The advantage of AFM in directly evaluating adhesion force lies in its ability to assess at a smaller scale compared with conventional contact angle methods, overcoming limitations related to large droplet volumes. AFM can use probes with radii of 20−40 nm to evaluate the adhesive properties between solids and liquids and quantitatively evaluate rocks by using different types of probes to obtain dominant mechanical actions.[43−45] Some AFM studies have evaluated the zeta potential of mineral surfaces and the mechanical curves of probe-wall interactions.[39−45] Atomic Force Microscopy (AFM) has been applied to the measurement of adhesion work in actual core samples. For instance, T. Hassenkam and colleagues[45] utilized an AFM probe to measure the chemical force maps of quartz sand particles extracted from sandstone in solutions of varying salinity. However, the direct application of AFM to shale samples remains relatively rare. This is primarily due to the extensive heterogeneity of shale samples, interference from organic matter, and challenges associated with the characterization of liquids and the quantification of subsequent adhesion levels. Therefore, this study qualitatively divided shale samples using scanning electron microscopy, defined experimental regions, measured basic physical properties, such as lithology and organic matter, and established quantitative characterization parameters.

In this study, building upon the scanning electron microscopy (SEM) results, roughness, and basic physical properties of rocks from previous research (the relevant data is cited in this article for readers to review directly[46]), we classified the rock surface into two characteristic regions: Bright Area (BA) and Dark Area (DA). This classification enabled us to identify the primary areas of roughness development and investigate the influence of different regions on contact angle results. These findings facilitate a direct discussion on the mechanisms and influencing factors of solid−liquid adhesion work. Based on this foundation, by using modified hydroxyl and gold−sulfur bond probes, we simulated the contact process between water-rock and oil-rock and analyzed the differences in water−solid/oil−solid adhesion work between different characteristic regions and the reasons for their generation. Subsequently, based on the adhesion work values obtained from probe rebound, we established a dimensionless adhesion work index I, which was used to evaluate the liquid-rock interactions at microscopic sites. The new wetting index reduces the influence of roughness on adhesion work expression, overcomes the shortcomings of traditional evaluation methods, and lays the foundation for further studying energy changes in the oil-rock detachment process.

https://doi.org/10.1021/acsomega.4c03682
ACS Omega 2024, 9, 30859−30872

Table 1. Inorganic and Organic Components of the Lucaogou Formation of JA and JB[46] (Reprinted in part, with permission from the publisher, cited from Ref 46. Copyright 2023 Energies.)

sample	quartz (%)	potassium feldspar (%)	plagioclase feldspar (%)	total clay content (%)	calcite (%)	dolomite (%)	TOC (%)
JA-3	32.8	9.2	27.7	14.8	4.3	11.2	3.64
JA-4	34.8	6.7	24.1	21.7	0.5	12.2	5.29
JA-6	47.3	13.6	20.5	3.5		15.1	5.18
JB-3	16.4	6.6	37.4	5.1	0.7	4.5	3.48
JB-4	19.9	7.2	51.8	3.4	0.5	17.6	2.71
JB-8	19.3	7.5	33	3.7		35.6	2.91

2. MATERIALS AND METHODS

2.1. Materials. The shale samples were obtained from wells JA and JB in the southeastern area of the Lucaogou (LCG) Formation in Jimusaer Sag, Xinjiang, China. The Jimusaer shale reservoir belongs to a mixed lithology type with a more complex mineral distribution compared to pure shale and interbedded shale. Therefore, it was necessary to conduct mineral analysis specifically for the samples required for this study. The results revealed that the minerals with relatively high content included quartz, potassium feldspar, sodium feldspar, and clay minerals, The test results are derived from our previous research,[46] as shown in Table 1.

We initially extracted 25 mm diameter cylindrical core samples from the full-diameter core. Subsequently, we controlled the sample thickness by using mechanical cutting methods. The cores underwent surface treatment using triple-beam argon ion polishing techniques (refer to Section 2.2 for specific procedures), resulting in samples with a smooth surface measuring 25 mm in diameter and 2 mm in thickness. These samples were prepared for scanning electron microscopy and atomic force microscopy measurements. Notably, the samples were preserved in their original state without undergoing oil washing processes, ensuring maximum integrity for subsequent analyses.

2.2. Preparation of Sample Flat Surfaces. The smooth surface of the samples underwent two processes: rough polishing and fine polishing, performed using the Leica mechanical thin sectioning machine and triple-beam argon ion polishing equipment. To eliminate scratches from mechanical cutting and achieve a flat surface, shale thin sections were sequentially polished under 9, 2, and 0.5 μm sandpapers. Subsequently, the samples underwent fine polishing using a triple-beam argon ion polishing system. The thin sections were alternately polished at voltages of 2 and 5 kV, each for 20 min per cycle, totaling 5 cycles, with a working current of 2 mA. The fine-polished samples aimed to minimize friction between the probe and sample surface during subsequent AFM measurements, thereby enhancing experimental precision.

2.3. AFM Measurements. In our study, we employed the PeakForce mode of atomic force microscopy (AFM), which is crucial for directly measuring adhesion work at nanoscale points. AFM offers three contact modes: contact mode, noncontact mode, and tapping mode, each providing valuable tools for surface analysis. The PeakForce mode, specifically utilized in our research, evaluates surface morphology and adhesion by detecting the vertical mechanical behavior of the probe on the shale surface.

AFM measurements were conducted using the tapping mode on each polished sample, with probes connected to the cantilever of the AFM instrument (Bruker, model Multimode8). The cantilever probe had an elastic constant (k) of 0.350 N/m, a resonance frequency (f0) of 65 kHz, and a tip radius of 30 nm. All measurements were performed at room temperature (296.15 K) and atmospheric pressure (1 atm) in ambient air. A typical scanning rate of 1 Hz was used during recording, with a maximum scan range of 100 μm × 100 μm. The height set point was configured at 200 nm, and PeakForce Quantitative Nanomechanical (QNM) mode was utilized to obtain surface topography information. The scanning area for the experiment was set at 20 μm × 20 μm.[46]

Following surface topography characterization, surface nanomechanical measurements were conducted using chemically modified hydrophobic/hydrophilic probes. Probes for adhesion work measurements underwent the following treatments: (1) for hydrophobic modification, the surface was treated with dodecanethiol, leading to the formation of gold−sulfur bonds between the thiol group and the gold-coated probe, resulting in the self-assembly of a monolayer connected to the AFM tip. (2) To achieve hydrophilicity and represent water−solid interface interactions, the AFM probe surface was modified with hydroxyl groups. Before each experiment, the probe was thoroughly rinsed with ethanol to remove any physically adsorbed substances, followed by nitrogen drying to prevent potential impacts of adsorbed materials on experimental data.

2.4. Contact Angle Measurement. In this study, we investigated the wetting properties of three adjacent points on the surface of each shale sample using the sessile drop method. The sessile drop method is one of the most widely used techniques for measuring contact angles. It involves placing a droplet of water (corresponding to the surface roughness measurement range mentioned later) on the marked positions on the solid sample surface using a pipet. High-speed cameras were used to capture the moment of contact between the solid−liquid interface and the liquid−air interface. This demonstrated the surface tension relationships between solid−gas, gas−liquid, and solid−liquid interfaces, as shown in Figure 1[46] (It is noteworthy that Figure 1 incorporates contact angle models under two types of roughness conditions: the Wenzel model in Figure 1b and the Cassie model in Figure 1c. The fundamental difference between them lies in whether air penetrates the rough surface). The coupled relationships based on the Young−Laplace equation can be expressed as follows:[34,35]

$$\cos\theta = \frac{\gamma_{sg} - \gamma_{sl}}{\gamma_{gl}} \quad (1)$$

where γ_{sg}, γ_{sl}, and γ_{gl} represent the surface tensions of the solid−gas, solid−liquid, and liquid−gas phases, respectively.

2.5. Other Tests. We conducted a series of conventional tests to characterize the physical properties of Jimusaer Lücaogou Formation shale samples, including scanning

https://doi.org/10.1021/acsomega.4c03682
ACS Omega 2024, 9, 30859−30872

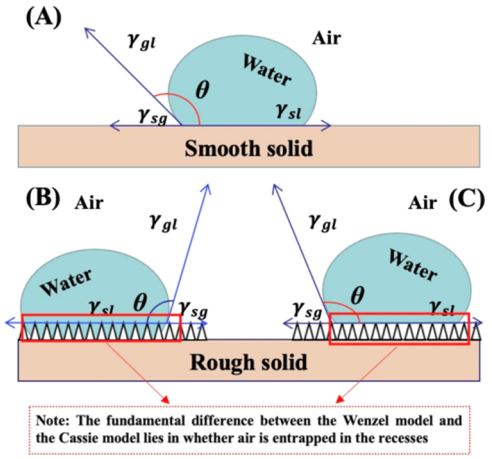

Figure 1. Relationship between contact angle and interfacial tension: (a) contact angle on a smooth surface, (b) Wenzel contact angle on a rough surface, and (c) Cassie contact angle on a rough surface[46] (Reprinted in part, with permission from the publisher, cited from Ref 46. Copyright 2023 Energies.).

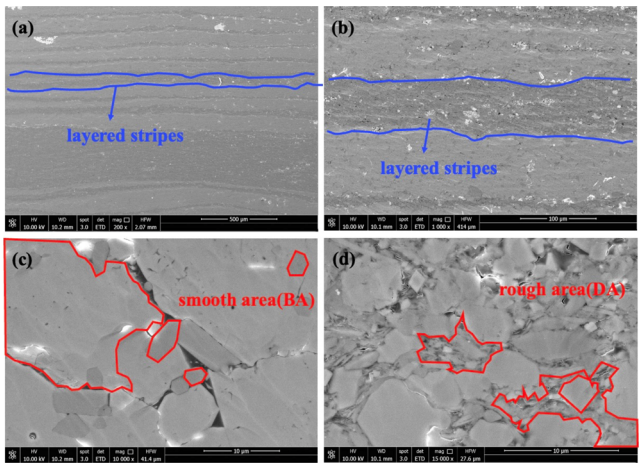

Figure 2. Development of Shale Laminations and Microscopic Images (panels (a) and (b) are sourced from Ref 46 (Reprinted in part, with permission from the publisher, cited from Ref 46. Copyright 2023 Energies.), while panels (c) and (d) are newly measured images. Additional images can be found in our previous research).

electron microscopy (SEM), high-pressure mercury intrusion, and low-temperature nitrogen adsorption experiments, this part of the study is consistent with our previous results.[46] (1) Through secondary electron scanning using SEM, we obtained images that display the surface rock features of the samples. These SEM images served as complementary tools for analyzing the surface roughness and adhesion properties. Within the designated marked areas, sample characteristics were precisely scanned under magnifications of 500, 100, and 10 μm. This detailed scanning formed the basis for sample feature classification and analysis, which includes identifying organic matter deposition areas and understanding the influence of mineral types on surface roughness. (2) Quantitative analysis of Jimusaer pore throat types was conducted by using high-pressure mercury intrusion and low-temperature nitrogen adsorption experiments. This laid the groundwork for investigating the impact of pore throat development on solid−liquid adhesion work on sample surfaces.

3. RESULTS

3.1. Scanning Electron Microscopy Results. After argon ion beam polishing, the samples underwent scanning electron microscopy (SEM) measurements, and the scanned images are displayed in Figure 2. From a broader perspective, Figure 2a,b[46] displays distinct stratified banding, a salient characteristic of the shale samples. These layers were formed under compression during the diagenesis process and are rich in organic matter, clay minerals, and a significant proportion of associated quartz. These zones are also the primary reservoirs of crude oil. Additionally, more measurements were conducted on the scanning electron microscope (SEM) images of shale samples at a smaller scale, as shown in Figure 2c,d. Upon zooming in from the 500 to 10 μm scale, numerous flat and rough surfaces were observed on the shale surface, indicating its unevenness and illustrating step-like development in the vertical direction, with the smooth portion identified as the Bright area (BA) and the rough portion as the Dark area (DA), as depicted in Figure 2c,d. This classification was previously discussed in our earlier research.[46]

Due to the limitations of optical microscopy in precisely determining the probe landing points during atomic force microscopy (AFM) measurements, it is imperative to classify the surface accordingly. The rough part appears black under the microscope, while the smooth surface appears brighter. Therefore, categorizing the samples into DA and BA facilitates the AFM measurements.

3.2. Contact Angle Measurement Results. The samples chosen for contact angle measurements exhibited hydrophobic properties, as shown in Table 2.[46] Sample JA displayed contact angles ranging from 121.3 to 133°, with an average of 125.3°, while sample JB showed contact angles ranging from 112.3 to 125°, with an average of 119°. These findings suggest that JB demonstrates relatively weaker hydrophobicity compared to JA. Importantly, the contact angle measurements revealed variations in solid−liquid adhesion characteristics across different points in the same sample. Previous research has highlighted the influence of surface roughness and mixed wetting distribution on contact angle results within the contact area. This variability in wetting behavior at the local level poses challenges in accurately describing solid−liquid adhesion properties. Macroscopic assessments may overlook the presence of oil droplets adhering to rough surfaces. Hence, a comprehensive understanding of adhesion necessitates considering both macroscopic and microscopic aspects, acknowledging the intricacies of wetting distribution at various scales,

Table 2. Results of Contact Angle Measurements[46] (Reprinted in part, with permission from the publisher, cited from Ref 46. Copyright 2023 Energies.)

sample	site 1	site 2	site 3	average
JA-3	129.3	124.1	133	128.8
JA-4	123.4	121.3	128.2	124.3
JA-6	121.7	124	122.9	122.9
average				125.3
JB-3	124.1	116.3	119.2	119.9
JB-4	112.3	121.3	113.2	115.6
JB-8	125	116.1	120.5	121.5
average				119

https://doi.org/10.1021/acsomega.4c03682
ACS Omega 2024, 9, 30859−30872

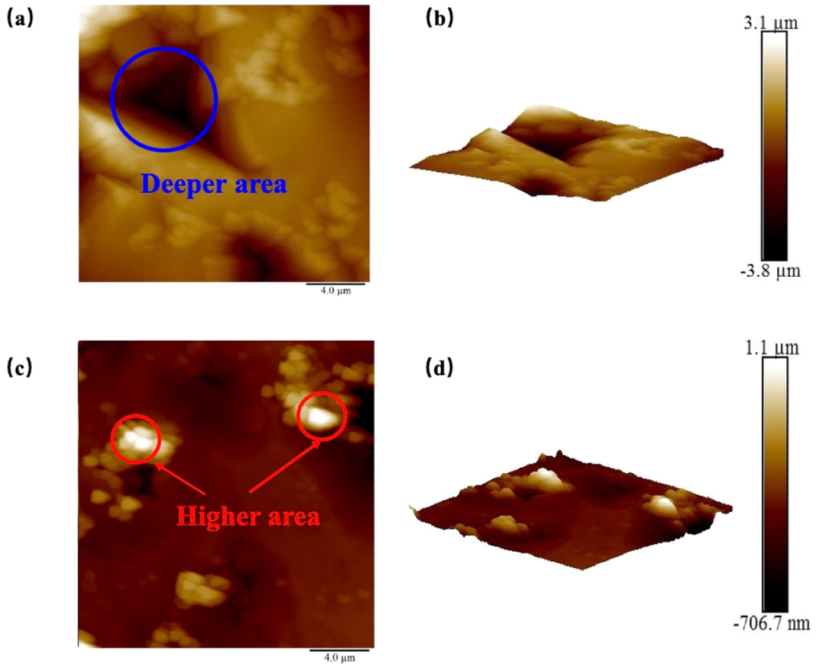

Figure 3. (a) 2D surface morphology image and (b) 3D surface morphology image of sample JA-3[46] (Reprinted in part, with permission from the publisher, cited from Ref 46. Copyright 2023 Energies.). (c) 2D surface morphology image and (d) 3D surface morphology image of sample JB-4.

identifying pertinent factors impacting adhesion characteristics, and minimizing measurement discrepancies.

3.3. Surface Roughness and Measurements. The surface roughness characteristics of the samples were assessed by using the contact mode of atomic force microscopy (AFM). AFM elucidates surface topography by repetitively scanning the probe along the axial direction, offering an effective means of analyzing surface roughness. As illustrated in the figures, both the 2D and 3D images depict fluctuations in the surface topography. These observations align with scanning electron microscopy (SEM) findings, indicating regions of the samples with diverse heights. Specifically, elevated regions tend to correspond to BA development, while lower areas correspond to DA development, in accordance with the discussion presented in Section 3.1 (Figure 3).

To quantify surface roughness, we selected R_a (average roughness) and R_q (root-mean-square roughness) as descriptors of surface heterogeneity. Specifically: (1) R_a represents the average deviation of surface profile lines from their mean value, indicating the degree of flatness or roughness in the horizontal (or vertical) direction. A smaller R_a value indicates a smoother surface; (2) R_q represents the root-mean-square value of surface roughness, reflecting the overall irregularity of surface profile fluctuations in the horizontal (or vertical) direction. A larger R_q value indicates a more irregular surface. The roughness results exhibited sample-specific characteristics, indicating that shale reservoirs do not develop according to a uniform roughness pattern. This variation is directly related to lithological development. For a detailed discussion, refer to our previous research (Table 3).

3.4. Adhesion Work Measurement Results by Atomic Force Microscopy. The adhesion work of the shale surface was measured using modified probes with measurements conducted on five points each from the BA/DA regions of each sample for water−solid adhesion work and oil−solid adhesion work, totaling 10 points. The average values of the measurement results are presented in Table 4.

Table 3. Surface Roughness of the Sample[46] (Reprinted in part, with permission from the publisher, cited from Ref 46. Copyright 2023 Energies.)

sample	R_a (nm)	R_q (nm)
JA-3	692	605
JA-4	529	647
JA-6	518	659
JB-3	114	170
JB-4	45.8	80.7
JB-8	123	195

The water−solid adhesion work ranges measured by AFM are as follows: (1) Within BA, JA: 0.742−3.104 nN/nm; JB: 0.72−0.852 nN/nm. (2) Within DA, JA: 2.788−13.184 nN/nm; JB: 3.098−5.276 nN/nm. The oil−solid adhesion work ranges are as follows: (1) Within BA, JA: 7.18−16.319 nN/nm; JB: 3.341−5.65 nN/nm. (2) Within DA, JA: 45.218−79.597 nN/nm. From the average values, both the water−solid and oil−solid adhesion work of JA are higher than those of JB, indicating that the JA well exhibits stronger attraction to water droplets/oil droplets. However, the results obtained from contact angle measurements only demonstrate the macroscopic oleophilic results and do not reflect the microscopic solid−liquid adhesion properties. Therefore, separately investigating the adhesion work between water/oil and rock is an important approach to understanding the liquid adsorption capacity of different areas of the Jimsar shale, as a detailed analysis will be provided in subsequent sections of the article.

4. DISCUSSION

4.1. Correlation between Contact Angle and Contact Angle Adhesion Work (W_c). Figure 4 illustrates the relationship between contact angle and W_c, and all three panels demonstrate a distinct negative correlation. This indicates that as the contact angle increases, the adhesion

https://doi.org/10.1021/acsomega.4c03682
ACS Omega 2024, 9, 30859−30872

Table 4. Results of Adhesion Work Measurement Using AFM

sample	solid−liquid adhesion work (DA)	solid−liquid adhesion work (BA)	solid−liquid adhesion work (average)	oil−solid adhesion work (DA)	oil−solid adhesion work (BA)	oil−solid adhesion work (average)
JA-3	2.788	0.742	1.765	45.2182	7.18	26.1991
JA-4	12.932	3.104	8.018	79.571	16.319	47.945
JA-6	13.184	2.678	7.931	59.01	15.622	37.316
average	9.63	2.17	5.90	61.27	13.04	37.15
JB-3	4.948	0.72	2.834	13.699	5.65	9.6745
JB-4	5.276	0.952	3.114	10.859	3.341	7.1
JB-8	3.098	0.8164	1.9572	28.652	4.654	16.653
average	4.44	0.83	2.64	17.74	4.55	11.14

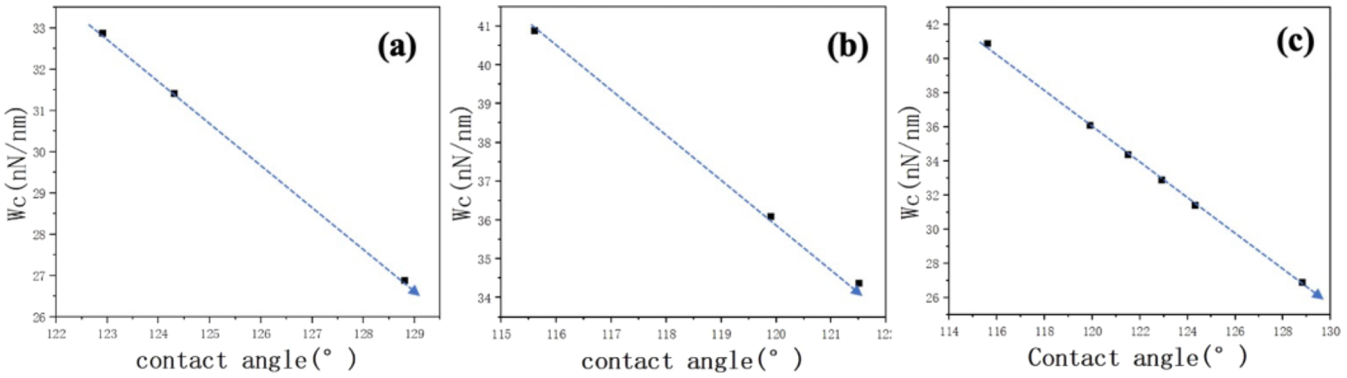

Figure 4. (a) Relationship between contact angle and contact angle adhesion work (W_c) for JA. (b) Relationship between contact angle and contact angle adhesion work (W_c) for JB. (c) Relationship between contact angle and contact angle adhesion work (W_c) for JA and JB.

between water droplets and the rock surface weakens, which is a fundamental property of wetting behavior.

The reasons for this phenomenon can be attributed to two factors: (1) the magnitude of the surface adhesion force and the contact area of water droplets. From the perspective of adhesion work, it reflects the merging capability between the two media. Therefore, when the attraction force of the solid substrate to the liquid is strong, more water droplets adhere to its surface. (2) The surface adhesion work is directly related to the solid−liquid contact area; the larger the contact area, the greater the surface adhesion work. To mitigate this effect, we kept the volume of the water droplets constant during the measurement process. However, there is still an interfering factor: surface roughness. When the sample surface is not smooth, the contact angle exhibits hysteresis. Hysteresis refers to the contact angle being in a nonsteady state, causing water droplets to shift or float on the rock surface, making the contact angle a dynamic value directly controlled by surface roughness.

However, the contact angle results do not directly reflect the size of the contact area (A). Therefore, we used the contact angle adhesion work (W_c) to demonstrate this phenomenon, and the calculation formula and results are as follows:

$$W_c = \sigma\ (1 + \cos\theta) \tag{2}$$

where σ represents the surface tension of water and θ is the contact angle.

Meanwhile, we derived the contact area between water droplets and solid surfaces based on the formulas for water droplet volume and surface area as follows:

$$A = \pi\left[\frac{3V}{\pi \tan^2\frac{\theta}{2}\left(\frac{3}{\sin\theta} - \tan\frac{\theta}{2}\right)}\right]^{2/3} \tag{3}$$

where V represents the volume of the water droplet.

The calculation results for W_c and A are listed in Table 5.

Table 5. W_c and Contact Area (A) of the Shale Samples

sample	JA-3	JA-4	JA-6	JB-3	JB-4	JB-8
W_c	26.885	31.427	32.891	36.108	40.890	34.387
A	10.615	12.211	12.722	13.810	15.429	13.230

The results in Figure 5 indicate a decreasing trend in the contact angle adhesion work with increasing surface roughness of the rock. However, it is noteworthy that the trends exhibited by the two wells are not the same, as shown in Figure 5, with slopes of −0.031 for (a) and −0.057 for (b). The curve for JB clearly shows a more pronounced slope, indicating a stronger influence of the water droplet adhesion on JB samples. From the perspective of solid−liquid adhesion, JB exhibits stronger hydrophilicity, meaning there are more hydrophilic sites at the microscopic scale provided by feldspar and clay minerals (for the relationship between mineral composition and roughness, refer to our previous study where it was found that the main contributors to roughness are TOC, quartz, and clay minerals, all belonging to DA[46]). However, the smooth surface of feldspar is not the primary source of roughness, leading our attention to focus on the rough clay minerals on the surface. As surface roughness increases, more air will enter DA, reducing the number of hydrophilic sites (clay mineral hydrophilicity) in JB samples compared to JA, thereby diminishing the

https://doi.org/10.1021/acsomega.4c03682
ACS Omega 2024, 9, 30859−30872

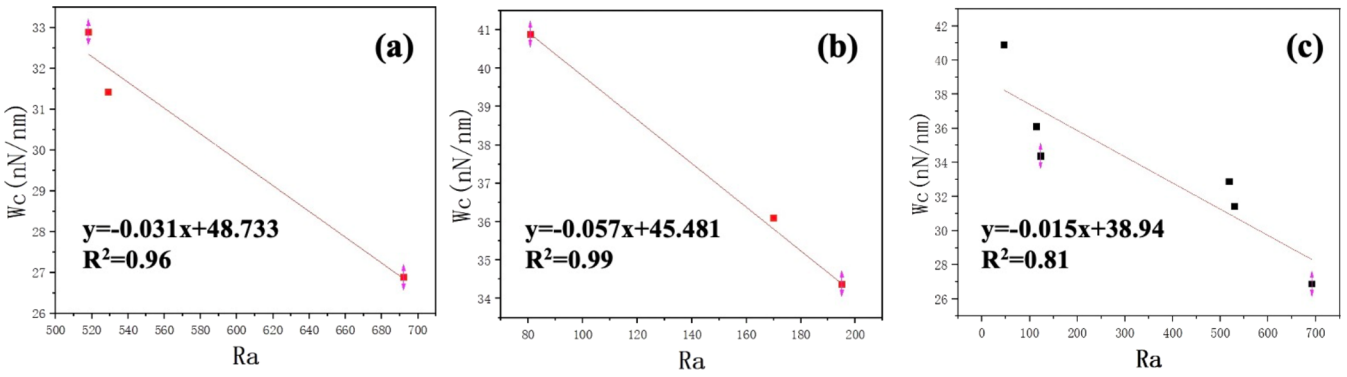

Figure 5. Relationship between surface roughness and W_c for (a) JA; (b) JB; and (c) JA and JB.

hydrophilic properties. Further discussion will be conducted in the next section.

4.2. Impact of Roughness on W_c. The roughness directly affects the solid−liquid contact area (A), showing a decreasing trend in A with increasing R_a, as seen in Figure 6, indicating

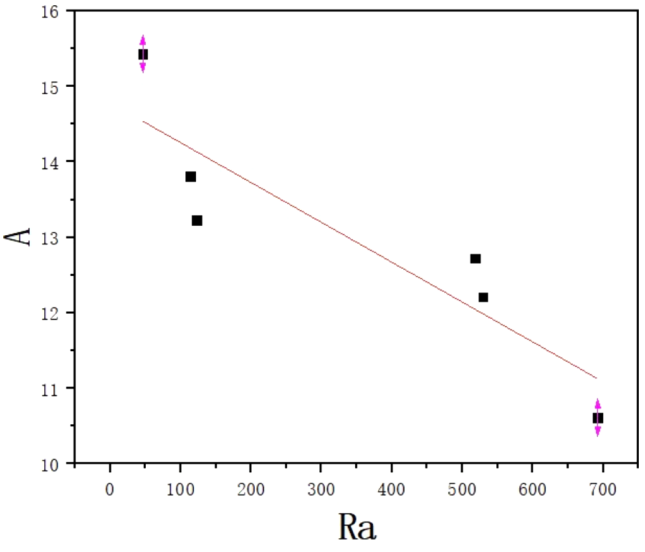

Figure 6. Correlation between R_a and A.

that air enters the uneven sample surface during contact angle measurements. This phenomenon reduces the contact area between water droplets and the sample surface. The macroscopic results do not fully reflect the microscopic distribution of wettability. Therefore, understanding how to mitigate the inhibitory effect of surface nonuniformity on wetting expression is essential for exploring the mutual attraction between solid and liquid phases.

Adhesion work is the product of the solid−liquid contact area and adhesion force, as indicated by the formula

$$W = FA \tag{4}$$

where F represents the magnitude of the unit adhesion force and A denotes the contact area.

When the contact area is equal to 1, the adhesion work directly represents the solid−liquid attraction per unit area. Therefore, multiplying the unit adhesion force by the unit area reflects the adhesion work per unit area between solid and liquid (denoted as W_{c1}).

The calculated results indicate that the unit adhesion work for JA ranges from 2.533 to 2.585 nN/nm, while for JB, it ranges from 2.599 to 2.615 nN/nm, with a maximum difference of 0.05. This effectively reduces the difference in adhesion work between the samples (Table 6), showing no significant positive or negative correlation with roughness, as shown in Figure 7.

Table 6. Adhesion Work Per Unit Area

sample	JA-3	JA-4	JA-6	JB-3	JB-4	JB-8
W_{c1}	2.533	2.574	2.585	2.615	2.650	2.599

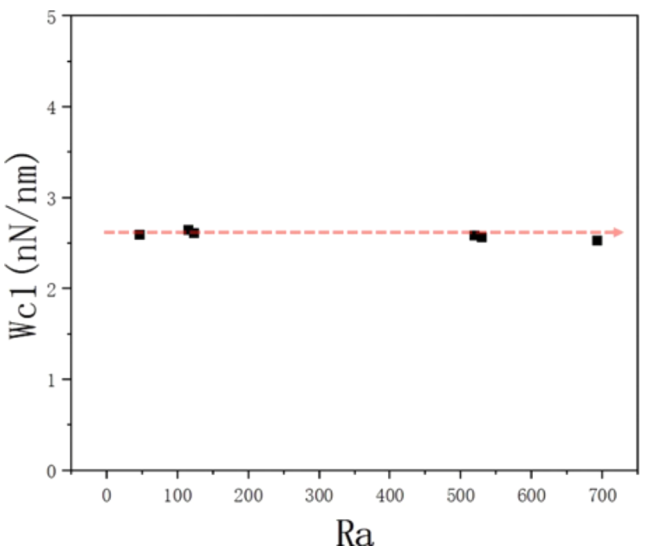

Figure 7. Relationship between surface roughness and unit adhesion work.

In order to further investigate the impact of roughness on the adhesion work of water droplets, this study utilized chemically treated AFM probes, whose tip radius of 20 nm effectively mitigated the influence of roughness. Adhesion work measurements were conducted in the nanometer scale on the samples, selecting 5 random points each in the BA and DA regions. The experimental results are listed in Table 4.

Clearly, water droplets exhibit stronger adhesion work in the DA region, indicating a decrease in DA development as the roughness decreases. This process compresses the area available for water droplet adhesion, leading to a decrease in the overall sample hydrophilicity. It is noteworthy that JA shows higher water adhesion work, but contact angle measurements present the opposite conclusion, which is attributed to oil-wet zone development. On a mixed-wetted

https://doi.org/10.1021/acsomega.4c03682
ACS Omega 2024, 9, 30859−30872

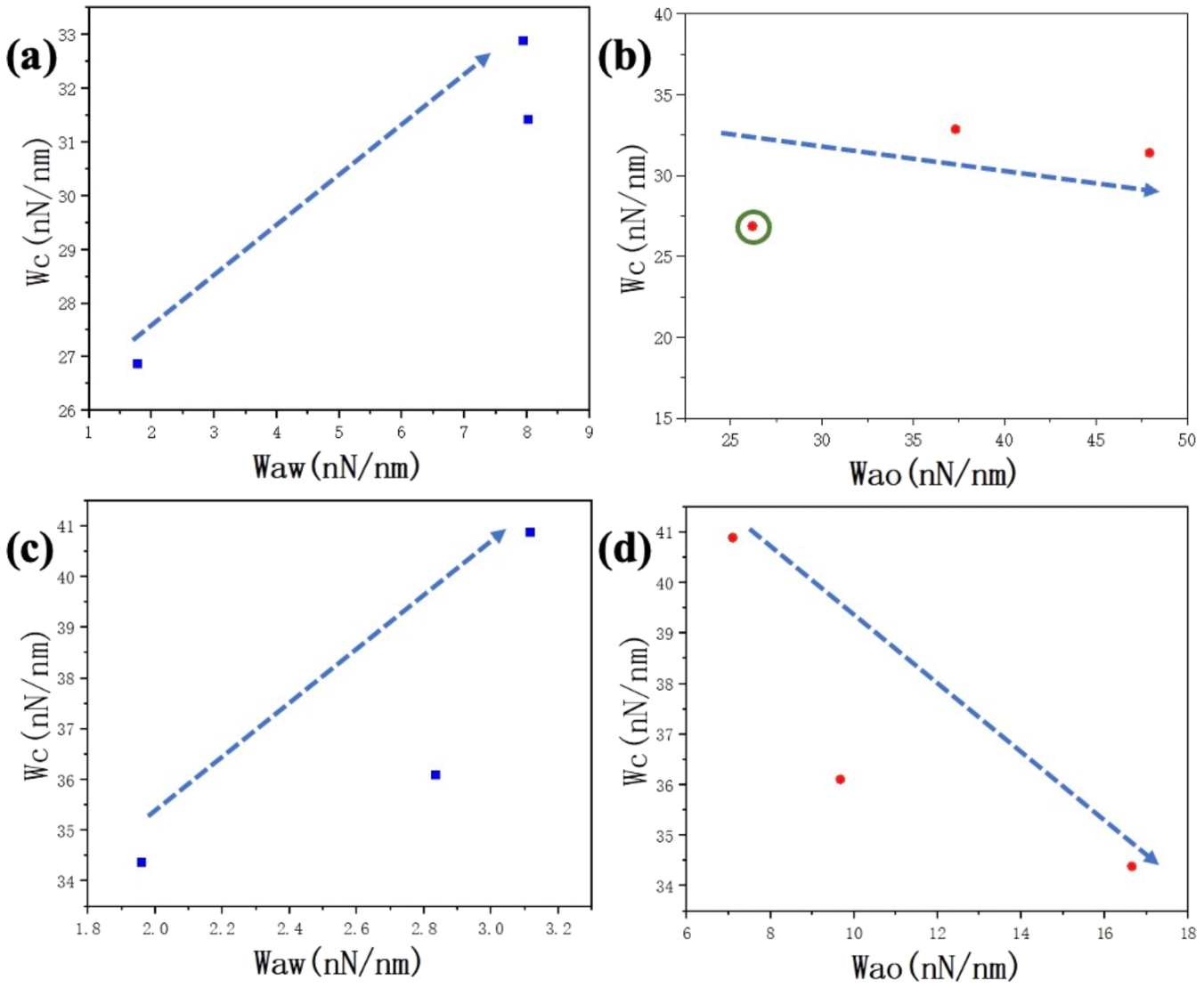

Figure 8. Relationship between hydrophilic probe measurements and W_c for (a) JA and (c) JB. Relationship between hydrophobic probe measurements and W_c for (b) JA and (d) JB.

core surface, the development of oil-wet points also affects the expression of surface adhesion properties. Therefore, we conducted a quantitative analysis of oil−solid adhesion work: the measurements revealed a stronger oil adhesion performance in DA, demonstrating that the adhesion force between water/oil is primarily provided by DA, attributed to the predominance of associated quartz, organic matter, and clay minerals. Quartz and organic matter are the main reasons for this phenomenon: (1) Quartz itself has hydrophilic properties, but this conclusion applies only to clean quartz surfaces; after oil aging is completed, quartz surfaces will undergo wetting modifications and exhibit oleophilic properties. Associated quartz develops in the fissures of large-grain rocks during formation processes, undergoing significant modifications during coexistence with organic matter. To authentically replicate subsurface rock surface characteristics, all tested samples underwent no oil washing process, preserving the oleophilic properties of modified quartz. (2) Organic matter is the original substance from which oil is generated, containing hydrocarbon substances not completely converted to oil and high-viscosity wax. They are considered part of the oil and, according to chemical compatibility principles, exhibit strong attraction to oil, significantly enhancing the rock's oleophilic properties. Relevant conclusions can be found in our previous studies and related articles investigating the wetting characteristics of samples before and after aging.[46−48]

To further demonstrate the impact of two different regions on the overall sample adhesion work, we discuss the relationship between W_a and W_c, as detailed in the next subsection.

4.3. Relationship between Adhesion Work of Contact Angle (W_c) and Adhesion Work of AFM (W_a). In this study, we established the correlation between roughness and adhesion work based on the data from Tables 3 and 4. Traditional contact angle results alone are insufficient to explain the influence of roughness on measurements, but adhesion work can directly reflect the impact of the contact area on the adhesion measurement process.

In this section, we discussed the influence of adhesion work in various regions on the overall adhesion capability of the samples and analyzed the modification process by organic matter on the samples (in the concluding part of this section). First, after quantitatively characterizing the oil/water adhesion work within BA and DA, we explored their correlation with W_c.

https://doi.org/10.1021/acsomega.4c03682
ACS Omega 2024, 9, 30859−30872

The trends shown in Figure 8 reveal two contrasting behaviors: the enhancement of water adhesion work (W_{aw}) promotes the development of overall hydrophilicity, while oil adhesion work (W_{ao}) exhibits the opposite trend. This validates the argument in Section 4.2 that dominance in oil wetness does not imply equal attraction capabilities of all points on the sample surface to crude oil; rather, it indicates that areas with strong oil wetness occupy more space. This development of oil wetness inhibits the formation of water wetness on rock surfaces, leading to a mixed wetting condition.[8,9] However, it is worth noting that there is an outlier in Figure 8b, where the W_{ao} of JA-3 is lower than the average level of the other samples, which is related to the degree of modification experienced by the rock. The primary space for crude oil in shale is in micropores.[49−51] To validate this point, we used comprehensive methods such as low-temperature nitrogen adsorption and high-pressure mercury intrusion to evaluate the size and distribution of pores in the shale, combined with scanning electron microscope images to investigate the development of pore throats in the target area. Micropores (<30 nm), small pores (30−200 nm), and intermediate pores (200−1500 nm) are the main pore types in Jimusaer shale, accounting for 53 and 7% of the total, respectively, representing the primary space for storing crude oil. The corresponding lithologies include: (1) small pores: quartz, potassium feldspar, and clay minerals; (2) micropores: quartz, potassium feldspar, clay minerals, and organic matter. Therefore, we conducted a proportional analysis of these minerals with specific results presented in Table 7:

Table 7. Proportion of Micropores, Small Pores, and Intermediate Pores

sample	JA-3	JA-4	JA-6	JB-3	JB-4	JB-8
intermediate pores	38.9	36.3	35.6	41.9	69.4	68.6
small pores	56.8	63.2	64.4	28.1	30.5	30.5
micropores	60.44	68.49	69.58	31.58	33.21	33.41

Microscopic pores and small pores in JA-3 have the lowest proportions, indicating a lesser influence from organic matter. Organic matter is considered to be a major contributor to oil wetting behavior. As emphasized by Siddiqui et al.,[52] organic compounds adsorbed on hydrophilic rock surfaces can lead to a transition from hydrophilic to oil-wet surfaces, ultimately exhibiting oil wetting characteristics in the pore structure of the rock. The presence of organic matter increases the complexity of shale wettability because the wettability of organic-rich shale is influenced by both mineral composition and organic matter. Therefore, compared to JA-4 and JA-6 with higher degrees of modification, JA-3 exhibits a relatively weaker oil wetting behavior. This phenomenon also applies to DA and BA, as shown in Figure 9.

Figure 9 depicts the trend of W_c with W_{ao} in BA and DA, which is consistent with Figure 8b,d, showing a negative correlation. This indicates that the overall wettability is constrained by local interactions between solid and liquid phases, and thus, the final wettability of the samples is a collection of numerous local oil-wet or water-wet sites. Additionally, panels (a) and (b) reveal that JA-3 exhibits lower oil wetting characteristics in both BA and DA, corresponding to areas modified by organic matter: (1) plagioclase, quartz (in the BA), and (2) organic matter, clay minerals, and quartz (in the DA). Areas with longer exposure to organic matter attachment are more likely to exhibit higher oil wetting characteristics. This is also one of the reasons for the differences observed in JA-3. As organic matter matures during strata development, the internal carboxyl groups and other oxygen-containing functional groups decrease, reducing the strong attraction with water molecules and deteriorating hydrophilicity, while aromatic rings and their aliphatic hydrocarbon chains increase, enhancing attraction with oil molecules and increasing oil wetting characteristics. As mentioned in our previous studies, this degree of modification is directly related to the content of organic matter. For more details, refer to the section on the correlation analysis between organic matter and minerals in Ref 46.[46]

Subsequently, we conducted an analysis of W_{aw} in different regions, as shown below:

Figure 10 illustrates the impact of W_{aw} in different regions on W_c. Both JA and JB exhibit the same trend in the BA and DA regions, indicating the contribution of local hydrophilicity to the overall hydrophilic adhesion work. As local hydrophilic adhesion work increases, the interactions between water and solid on the sample surface intensify, resulting in more hydrophilic sites on the sample surface and, thus, higher hydrophilicity.

Therefore, characterizing the solid−liquid adhesion properties in local regions can effectively reflect the wettability of the overall sample. However, a single measurement of water−solid/oil−solid adhesion cannot accurately quantify and compare the wettability differences between shale samples. To address this, we established a normalized adhesion work index to explore the influence of roughness on adhesion work expression. Refer to the next section for details.

4.4. Quantitative Characterization of Local Wettability and Overall Wettability. To quantitatively assess the adsorption level of rocks to crude oil/water droplets, we conducted a fitting analysis of the difference and sum of oil−water adhesion work values and proposed an evaluation method based on AFM. By coupling the adhesion work at the oil−solid interface and the water−solid interface, we established a dimensionless wettability index, denoted as I, to differentiate the adhesion levels of different samples to water droplets/crude oil. The specific formula is as follows:

$$I = \frac{W_{os} - W_{ws}}{W_{os} + W_{ws}} \tag{5}$$

where W_{os} represents the adhesion work between oil and solid and W_{ws} represents the adhesion work between water and solid. When $0 \le I \le 1$, the sample is considered oil-wet, whereas when $-1 \le I < 0$, the sample is considered water-wet. Since the wettability index is normalized, its maximum value is 1. This evaluation method also applies to water-wet cores with a wettability index less than 0.

The adhesion capabilities of different samples to oil/water were evaluated using the newly established AFM evaluation method. The results are shown in Table 8, where significant differences in adhesion behavior between hydrophobic and hydrophilic surfaces are highlighted, emphasizing the comparison of oil-rock/water-rock interactions, which form the basis of nanomechanical wettability assessment. The results indicate that the average indices of each core sample are all less than 1. Additionally, to facilitate comparison with the results from the contact angle method, the dimensionless contact angle results

https://doi.org/10.1021/acsomega.4c03682
ACS Omega 2024, 9, 30859−30872

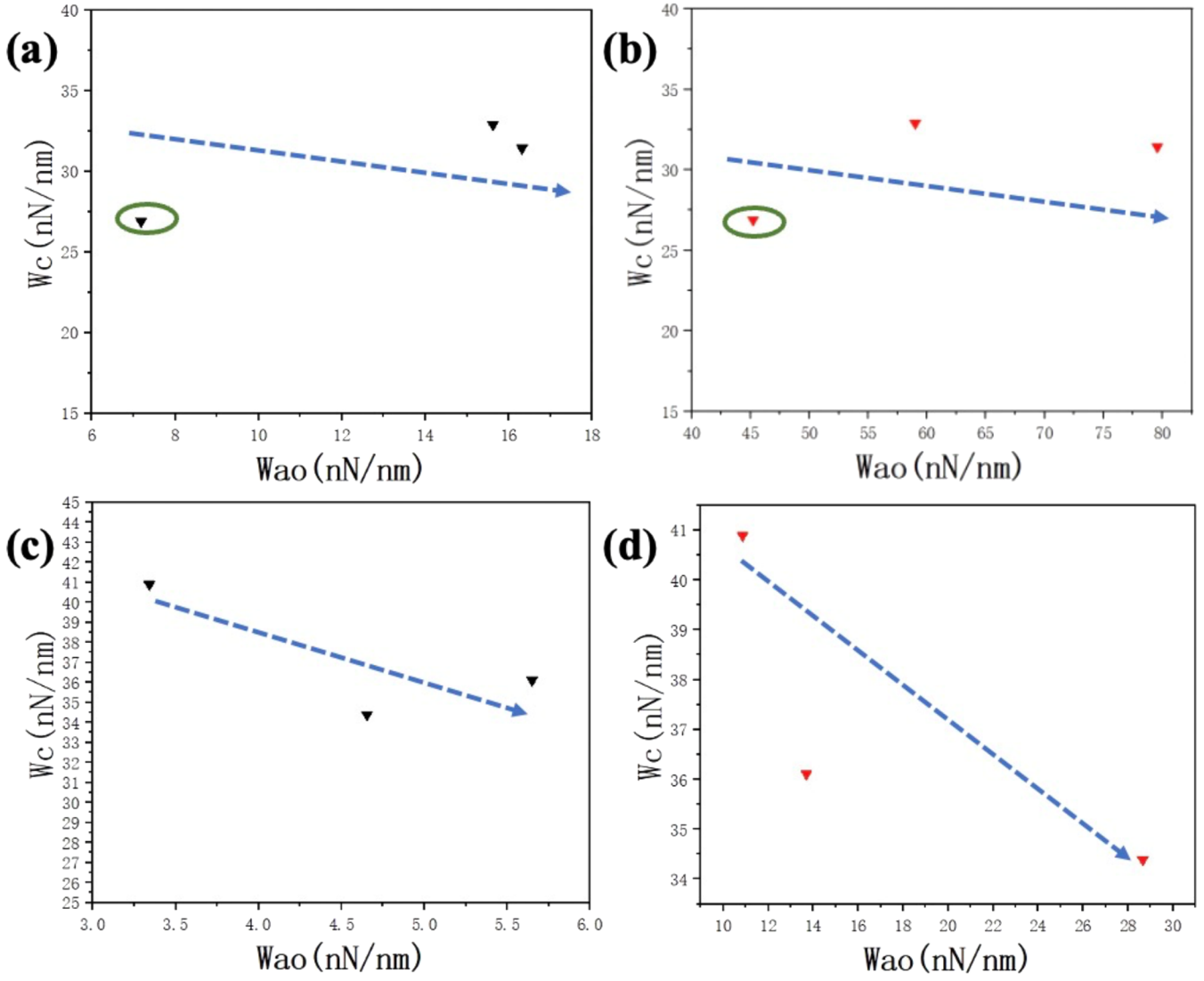

Figure 9. Correlation between W_{ao} and W_c for JA: (a) BA and (b) DA, and JB: (c) BA and (d) DA.

were normalized and denoted as C, converted into dimensionless indices ranging from −1 to 1, When $0 \leq C \leq 1$, the sample is considered to be oil-wet; when $-1 \leq C < 0$, it is considered to be water-wet, as shown in Table 8.

$$C = \frac{\theta - 90^{\circ}}{90^{\circ}} \tag{6}$$

The results indicate that the values of I are greater than those of C, and there is a good correlation between I and C, as well as between I and the contact angle (CA), as shown in Figure 11. The correlation coefficients between I and CA for the two wells are 0.99 and 0.86, respectively, while those between I and C are also 0.99 and 0.86, respectively. Considering the data from the two wells, the correlation indices are 0.813 and 0.813, respectively. These two sets of data can be discussed in two aspects: (1) In both wells, C and CA exhibit the same correlation with I, with R^2 values of 0.99 and 0.86, respectively, indicating that the normalized index C can be used for further analysis. (2) The positive correlation trend in Figure 11 indicates the influence of heterogeneity on contact angle measurements. After the influence of rock heterogeneity is avoided (using AFM measurements), the adhesion performance of the sample surface is expressed, and the shale samples from the target block exhibit strong oil wettability, indicating the existence of uncontacted areas between water droplets and rocks. This phenomenon significantly affects the assessment of the adhesion properties. Taking the target block in this study as an example, enhanced rock heterogeneity weakens the expression of sample oil wettability, exposing only partial areas of oil−solid adhesion and failing to fully demonstrate the strong oil wettability of DA, leading to measurement errors.

Regarding the phenomenon of JB having a lower correlation coefficient than JA, we conducted an analysis based on mineral composition and pore development (large pores mainly exist in the form of intergranular dissolution pores + residual intergranular pores, with a low content and no clear relationship with the roughness caused by minerals, which is not discussed in this paper). The main pores developed in JB are medium-sized pores, mainly developed in plagioclase and calcite (with relatively flat surfaces). From the perspective of mineral content (Table 1), these two minerals account for 41.9, 69.4, and 68.6% of pore development, respectively, which are higher than the development of micropores in each sample (31.58, 33.21, and 33.41%, respectively). This results in more oil-wet spaces in BA and reduces DA, i.e., reducing the

https://doi.org/10.1021/acsomega.4c03682
ACS Omega 2024, 9, 30859−30872

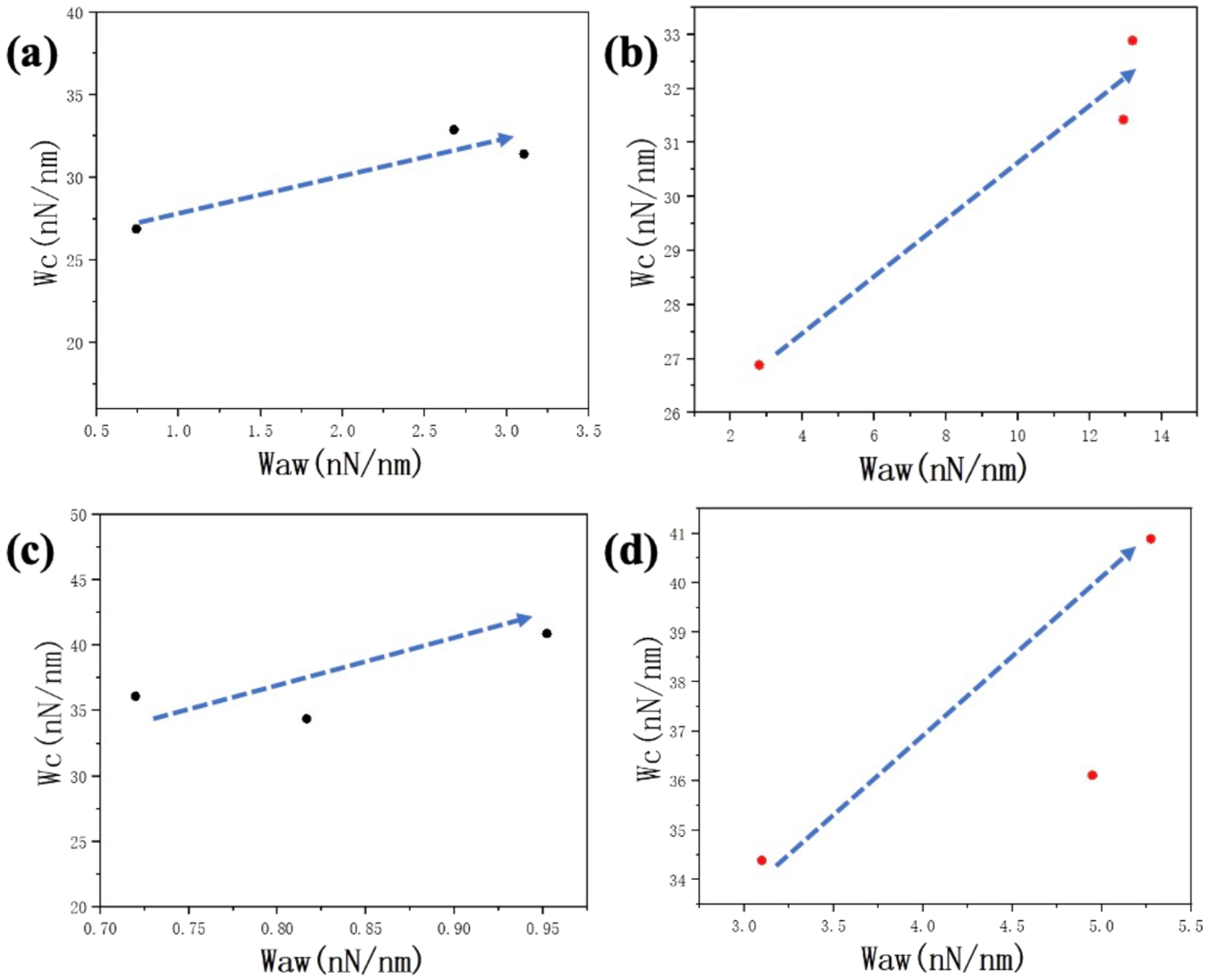

Figure 10. Correlation between W_{aw} and W_c for JA: (a) BA and (b) DA, and JB: (c) BA and (d) DA.

Table 8. Results of *I* and *C*

sample	JA-3	JA-4	JA-6	JB-3	JB-4	JB-8
I	0.874	0.713	0.649	0.547	0.390	0.790
C	0.431	0.381	0.366	0.332	0.284	0.350

influence of rougher areas on the contact angle method. Therefore, the lower correlation coefficient is due to JB having a higher proportion of medium-sized pores compared with JA, which is dominated by micropore development.

Considering both JA (discussed at the end of Section 4.3) and JB wells comprehensively, the increase in the proportion of pore development in BA within JB indeed enhances the expression of oil wetting. This is evident from the difference in oil−solid adhesion work between BA and DA in JB compared with JA, as shown in Table 9. The difference in oil−solid adhesion work between BA and DA in JB is smaller than in JA, indicating that with the development of medium-sized pores in JB, the areas within the bright zones undergo stronger oil modification, reducing the difference in oil−solid adhesion work between the two regions.

5. CONCLUSIONS

The paper discusses the causes of roughness in the Lucaogou shale reservoir of the Jimsar Formation and solid−liquid adhesion. Based on the contact angle method and AFM, the paper explores the impact of rock heterogeneity on liquid adhesion processes, clarifying the role of pore development in surface modification and proposing an adhesion evaluation index I that is not affected by roughness. The specific conclusions are as follows:

(1) The correlation between water−solid contact area and surface roughness is discussed. With the enhancement of surface heterogeneity, more air enters the high and low uneven grooves, hindering the contact between water droplets and the wall surface, reducing the contact area between water and solid, and making the oil/water affinity unable to be fully expressed.

https://doi.org/10.1021/acsomega.4c03682
ACS Omega 2024, 9, 30859−30872

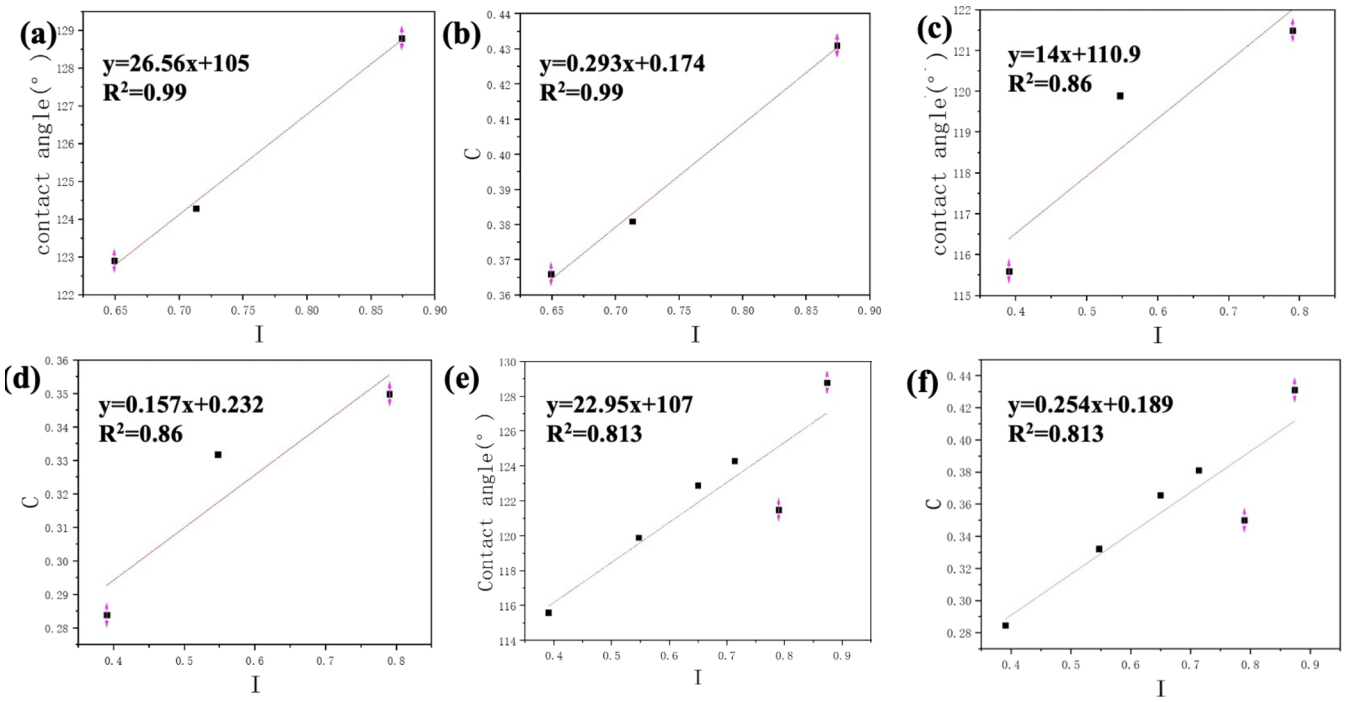

Figure 11. Correlation between JA: (a) *I* and CA, and (b) *I* and *C*, and JB: (c) *I* and CA, and (d) *I* and *C*, and JA and JB: (e) *I* and CA, and (f) *I* and *C*.

Table 9. Differences in Oil−Solid Adhesion Work between DA and BA for JA and JB

sample	JA-3	JA-4	JA-6	JB-3	JB-4	JB-8
the difference in oil−solid adhesion work between BA and DA	38.0382	63.252	43.388	8.049	7.518	23.998

(2) It is clarified that the roughness of the Jimsar samples is mainly contributed by DA, which contains a large amount of quartz, organic matter, and clay minerals. Due to the presence of organic matter, this part exhibits strong oil−solid adhesion compared to BA, making it one of the main contributing areas to sample oil wettability.

(3) Due to the fact that pores are the main reservoir spaces for shale oil, their development characteristics directly impact the distribution of surface oil wettability. As discussed in Sections 4.3 and 4.4, when samples are primarily developed with micropores, the oil wettability of shale DA is stronger; when samples are primarily developed with mesopores, BA's oil wettability is enhanced. This phenomenon also reduces the impact of roughness on the expression of oil wettability in JB wells.

(4) Based on AFM measurement results, an evaluation parameter *I* was established to characterize solid−liquid adhesion, minimizing the influence of roughness on adhesion evaluation, and showing a good correlation with *C*/CA. Therefore, evaluation index *I* can be used to distinguish and analyze the differences in liquid−solid adhesion between different samples.

AUTHOR INFORMATION

Corresponding Author

Linghui Sun − *Engineering College, University of Chinese Academy of Sciences, Beijing 100190, China; Institute of Porous Flow and Fluid Mechanics, Chinese Academy of Sciences, Beijing 100083, China; Research Institute of Petroleum Exploration and Development, Petrochina, Beijing 100083, China*; Email: sunlinghuipetro@163.com

Authors

Xu Huo − *Engineering College, University of Chinese Academy of Sciences, Beijing 100190, China; Institute of Porous Flow and Fluid Mechanics, Chinese Academy of Sciences, Beijing 100083, China*; orcid.org/0009-0005-7693-1084

Feiyu Chen − *Engineering College, University of Chinese Academy of Sciences, Beijing 100190, China; Institute of Porous Flow and Fluid Mechanics, Chinese Academy of Sciences, Beijing 100083, China*; orcid.org/0009-0001-5832-8688

Zhengming Yang − *Engineering College, University of Chinese Academy of Sciences, Beijing 100190, China; Institute of Porous Flow and Fluid Mechanics, Chinese Academy of Sciences, Beijing 100083, China; Research Institute of Petroleum Exploration and Development, Petrochina, Beijing 100083, China*

Xiuxiu Pan − *Engineering College, University of Chinese Academy of Sciences, Beijing 100190, China; Institute of Porous Flow and Fluid Mechanics, Chinese Academy of Sciences, Beijing 100083, China*; orcid.org/0009-0003-9226-3843

Junqian Li − *School of Geosciences, China University of Petroleum (East China), Qingdao 266580, China*; orcid.org/0000-0001-8854-3373

Zhaojing Song − *School of Geosciences, China University of Petroleum (East China), Qingdao 266580, China*

https://doi.org/10.1021/acsomega.4c03682
ACS Omega 2024, 9, 30859−30872

Zhirong Zhang − *Engineering College, University of Chinese Academy of Sciences, Beijing 100190, China; Institute of Porous Flow and Fluid Mechanics, Chinese Academy of Sciences, Beijing 100083, China*

Chun Feng − *Research Institute of Petroleum Exploration and Development, Petrochina, Beijing 100083, China*

Complete contact information is available at: https://pubs.acs.org/10.1021/acsomega.4c03682

Notes

The authors declare no competing financial interest.

REFERENCES

(1) Wang, M.; Li, M.; Li, B.; Liang, X.; Jinxu, Z.; et al. The key parameter of shale oil resource evaluation: Oil content. *Pet. Sci.* **2022**, *19* (4), 1443−1459, DOI: 10.1021/acsomega.2c03393.

(2) Hu, T.; Pang, X.; Jiang, F.; Wang, Q.; Liu, X.; Wang, Z.; Jiang, S.; Wu, G.; Li, C.; Xu, T.; et al. Movable oil content evaluation of lacustrine organic-rich shales: Methods and a novel quantitative evaluation model. *Earth-Sci. Rev.* **2021**, *214*, No. 103545, DOI: 10.1016/j.earscirev.2021.103545.

(3) Caineng, Z.; Feng, M.; Songqi, P.; Xinshun, Z.; Songtao, W.; Guoyou, F.; Hongjun, W.; Zhi, Y. Formation and distribution potential of global shale oil and the developments of continental shale oil theory and technology in China. *Earth Sci. Front.* **2023**, *30* (1), No. 128.

(4) Wang, M.; Ma, R.; Li, J.; Shuangfang, L.; Chuanming, L.; Zhiqiang, G.; Zheng, L. Occurrence mechanism of lacustrine shale oil in the Paleogene Shahejie Formation of Jiyang depression, Bohai Bay Basin, China. *Pet. Explor. Dev.* **2019**, *46* (4), 833−846, DOI: 10.1016/s1876-3804(19)60242-9.

(5) Kelai, X.; Zhang, Y.; Yingchang, C.; Gong, J.; Li, K.; Lin, M. Control of micro-wettability of pore-throat on shale oil occurrence: A case study of laminated shale of Permian Lucaogou Formation in Jimusar Sag, Junggar Basin, NW China. *Pet. Explor. Dev.* **2023**, *50* (2), 334−345, DOI: 10.1016/s1876-3804(23)60391-x.

(6) AlRatrout, A.; Blunt, M. J.; Bijeljic, B. Wettability in complex porous materials, the mixed-wet state, and its relationship to surface roughness. *Proc. Natl. Acad. Sci. U.S.A.* **2018**, *115* (36), 8901−8906.

(7) Deglint, H. J.; Clarkson, C. R.; Ghanizadeh, A.; DeBuhr, C.; Wood, J. M. Comparison of micro-and macro-wettability measurements and evaluation of micro-scale imbibition rates for unconventional reservoirs: Implications for modeling multi-phase flow at the micro-scale. *J. Nat. Gas Sci. Eng.* **2019**, *62*, 38−67, DOI: 10.1016/j.jngse.2018.11.026.

(8) Lv, X.; Sun, J.; Liao, B.; Chaoqiang, F.; Kaihe, L.; Zhangxin, C.; Jintang, W.; Jinsheng, S.; Peng, C.; Xiaojuan, S. The effect of mixed wettability on flow characteristics in porous media of ultra-deep gas reservoirs: Molecular dynamics simulations and numerical simulations. *Appl. Surf. Sci.* **2024**, *654*, No. 159541, DOI: 10.1016/j.apsusc.2024.159541.

(9) AlOmier, A.; Cha, D.; Ayirala, S.; Ali, A.; Hussein, H. Novel fabrication of mixed wettability micromodels for pore-scale studies of fluid−rock interactions. *Lab Chip* **2024**, *24* (4), 882−895, DOI: 10.1039/d3lc01009k.

(10) Nguyen, D.; Phan, T.; Hsu, T. P.; Phan, J. Adhesion and surface energy of shale rocks. *Colloids Surf., A* **2017**, *520*, 712−721.

(11) Mirchi, V.; Soheil, S.; Lamia, Goual.; Mohammad, P. Dynamic interfacial tension and wettability of shale in the presence of surfactants at reservoir conditions. *Fuel* **2015**, *148*, 127−138.

(12) Mirchi, V.; Saraji, S.; Goual, L.; Piri, M. *Dynamic Interfacial Tensions and Contact Angles of Surfactant in Brine/Oil/Shale Systems: Implications to Enhanced Oil Recovery in Shale Oil Reservoirs*. In SPE Improved Oil Recovery Symposium, SPE-169171-MS, 2014.

(13) Van Oss, C.; Good, R. J.; Chaudhurry, M. Additive and nonadditive surface tension components and interpretation of contact angles. *Langmuir* **1988**, *4*, 884−891, DOI: 10.1021/la00082a018.

(14) Van Oss, C.; Chaudhurry, M.; Good, R. J. Interfacial Lifshitz-van der Waals and polar interactions in macrospic systems. *Chem. Rev.* **1988**, *88*, 927−941, DOI: 10.1021/cr00088a006.

(15) Stammitti-Scarpone, A.; Acosta, E. J. Solid-liquid-liquid wettability and its prediction with surface free energy models. *Adv. Colloid Interface Sci.* **2019**, *264*, 28−46.

(16) Clint, J. H. Adhesion and components of solid surface energies. *Curr. Opin. Colloid Interface Sci.* **2001**, *6* (1), 28−33.

(17) Ferrari, J. V.; de Oliveira Silveira, B. M.; Arismendi-Florez, J. J.; Fagundes, T. B.; da Trindade Silva, M. A.; Skinner, R.; Ulsen, C.; de Carvalho, C. C. Influence of carbonate reservoir mineral heterogeneities on contact angle measurements. *J. Pet. Sci. Eng.* **2021**, *199*, No. 108313, DOI: 10.1016/j.petrol.2020.108313.

(18) Cappella, B.; Stark, W. Adhesion of amorphous polymers as a function of temperature probed with AFM force−distance curves. *J. Colloid Interface Sci.* **2006**, *296* (2), 507−514.

(19) Lyu, Y.; Huang, Q.; Li, R.; Zhang, F.; Liu, L.; Zhang, H.; Zhang, Y.; Cui, Y.; Wang, Q. Effect of temperature on wall sticking of heavy oil in low-temperature transportation. *J. Pet. Sci. Eng.* **2021**, *206*, No. 108944.

(20) Serro, A. P.; Colaço, R.; Saramago, B. Adhesion forces in liquid media: Effect of surface topography and wettability. *J. Colloid Interface Sci.* **2008**, *325* (2), 573−579.

(21) Jagadisan, A.; Heidari, Z. Impacts of competitive water adsorption of kerogen and clay minerals on wettability of organic-rich mudrocks. *SPE Reservoir Eval. Eng.* **2020**, *23* (04), 1180−1189, DOI: 10.2118/201202-PA.

(22) Zdziennicka, A.; Szymczyk, K.; Jańczuk, B. Correlation between surface free energy of quartz and its wettability by aqueous solutions of nonionic, anionic and cationic surfactants. *J. Colloid Interface Sci.* **2009**, *340* (2), 243−248.

(23) Laird, D. A. Layer charge influences on the hydration of expandable 2:1 phyllosilicates. *Clays Clay Miner.* **1999**, *47* (5), 630−636.

(24) Shi, K. Y.; Chen, J. Q.; Pang, X. Q.; Jiang, F. J.; Hui, S. S.; Zhao, Z. C.; Chen, D.; Cong, Q.; Wang, T.; Xiao, H. Y.; et al. Wettability of different clay mineral surfaces in shale: Implications from molecular dynamics simulations. *Pet. Sci.* **2023**, *20* (2), 689−704, DOI: 10.1016/j.petsci.2023.02.001.

(25) Noruzi, Y.; Sharifi, M.; Fahimpour, J.; Sabet, M.; Akbari, M.; Hosseini, S. The state-of-the-art of wettability alteration in sandstones and carbonates: A mechanistic review. *Fuel* **2024**, *356*, No. 129570.

(26) Deng, X.; Patil, S.; Kamal, M. S.; Mahmoud, M.; Sultan, A.; Saikia, T. Wettability alteration of carbonate rock by chelating agents and viscoelastic surfactants: synergetic impact. *Energy Fuels* **2022**, *36* (14), 7391−7401.

(27) Bakhshi, E.; Torab, F. M. Determining wettability of fractured carbonate reservoirs. *Nat. Resour. Res.* **2016**, *25*, 211−225, DOI: 10.1007/s11053-015-9282-z.

(28) Aftab, A.; Ali, M.; Altaf, M.; Sarmadivaleh, M. Influence of stearic acid and alumina nanofluid on CO_2 wettability of calcite substrates: Implications for CO_2 geological storage in carbonate reservoirs. *J. Colloid Interface Sci.* **2023**, *646*, 567−575, DOI: 10.1016/j.jcis.2023.05.066.

(29) Shi, C.; Xie, L.; Zhang, L.; Lu, X.; Hongbo, Z. Probing the interaction mechanism between oil droplets with asphaltenes and solid surfaces using AFM. *J. Colloid Interface Sci.* **2020**, *558*, 173−181, DOI: 10.1016/j.jcis.2019.09.092.

(30) Taqvi, S. T.; Almansoori, A.; Bassioni, G. Understanding the role of asphaltene in wettability alteration using ζ potential measurements. *Energy Fuels* **2016**, *30* (3), 1927−1932.

(31) Rocha, J. A.; Baydak, E. N.; Yarranton, H. W.; Sztukowski, D. M.; Ali, M. V.; Gong, L.; Shi, C.; Zeng, H. Role of aqueous phase chemistry, interfacial film properties, and surface coverage in stabilizing water-in-bitumen emulsions. *Energy Fuels* **2016**, *30* (7), 5240−5252, DOI: 10.1021/acs.energyfuels.6b00114.

(32) Salou, M.; Siffert, B.; Jada, A. Interfacial characteristics of petroleum bitumens in contact with acid water. *Fuel* **1998**, *77* (4), 343−346.

(33) Cwickel, D.; Paz, Y.; Marmur, A. Contact angle measurement on rough surfaces: the missing link. *Surf. Innovations* **2017**, *5* (4), 190−193, DOI: 10.1680/jsuin.17.00021.
(34) Zhu, M.; Liu, Y.; Chen, M.; Xu, Z.; Li, L.; Zhou, Y. Metal mesh-based special wettability materials for oil-water separation: A review of the recent development. *J. Pet. Sci. Eng.* **2021**, *205*, No. 108889.
(35) Wenzel, R. N. Resistance of solid surfaces to wetting by water. *Ind. Eng. Chem.* **1936**, *28* (8), 988−994, DOI: 10.1021/ie50320a024.
(36) Wu, Y.; Luo, Q.; Chu, Z.; Linghui, S.; Xin, S.; Zijia, L.; Wenbo, R.; Bin, Y. Microscale Reservoir Wettability Evaluation Based on Oil−Rock Nanomechanics. *Energy Fuels* **2023**, *37* (9), 6697−6704, DOI: 10.1021/acs.energyfuels.3c00799.
(37) Koetniyom, W.; Suhatcho, T.; Treetong, A.; Thiwawong, T. AFM force distance curve measurement for surface investigation of polymers compound blend with metal nanoparticles. *Mater. Today: Proc.* **2017**, *4* (5), 6205−6211.
(38) Luo, Y.; Andersson, S. B. A continuous sampling pattern design algorithm for atomic force microscopy images. *Ultramicroscopy* **2019**, *196*, 167−179.
(39) Lu, Y.; Liu, D.; Cai, Y.; Gao, C.; Jia, Q.; Zhou, Y. AFM measurement of roughness, adhesive force and wettability in various rank coal samples from Qinshui and Junggar basin, China. *Fuel* **2022**, *317*, No. 123556.
(40) Liu, F.; Yang, H.; Wang, J.; Minghui, Z.; Ting, C.; Guangxin, H.; Wei, Z.; Jiangzhong, W.; Shijing, X.; Xu, Wu.; et al. Salinity-dependent adhesion of model molecules of crude oil at quartz surface with different wettability. *Fuel* **2018**, *223*, 401−407, DOI: 10.1016/j.fuel.2018.03.040.
(41) Liu, S.; Xie, L.; Liu, J.; Guangyi, L.; Hong, Z.; Yixiang, W.; Hongbo, Z. Probing the interactions of hydroxamic acid and mineral surfaces: Molecular mechanism underlying the selective separation. *Chem. Eng. J.* **2019**, *374*, 123−132, DOI: 10.1016/j.cej.2019.05.152.
(42) Wang, J.; Li, J.; Xie, L.; Shi, C.; Qingxia, L.; Hongbo, Z. Interactions between elemental selenium and hydrophilic/hydrophobic surfaces: Direct force measurements using AFM. *Chem. Eng. J.* **2016**, *303*, 646−654, DOI: 10.1016/j.cej.2016.06.039.
(43) Stevens, R. M. New carbon nanotube AFM probe technology. *Mater. Today* **2009**, *12* (10), 42−45.
(44) Pedersen, N. R.; Hassenkam, T.; Ceccato, M.; Dalby, K. N.; Mogensen, K.; Stipp, S. L. S. Low salinity effect at pore scale: probing wettability changes in Middle East limestone. *Energy Fuels* **2016**, *30* (5), 3768−3775.
(45) Matthiesen, J.; Hassenkam, T.; Bovet, N.; Dalby, K. N.; Stipp, S. L. S. Adsorbed organic material and its control on wettability. *Energy Fuels* **2017**, *31* (1), 55−64.
(46) Xu, H.; Linghui, S.; Zhengming, Y.; Junqian, L.; Chun, F.; Zhirong, Z.; Xiuxiu, P.; Meng, D. Mechanism and Quantitative Characterization of Wettability on Shale Surfaces: An Experimental Study Based on Atomic Force Microscopy (AFM). *Energies* **2023**, *16* (22), No. 7527, DOI: 10.3390/en16227527.
(47) Huang, J.; Stoyanov, S. R.; Zeng, H. A comparison study on adsorption and interaction behaviors of diluted bitumen and conventional crude oil on model mineral surface. *Fuel* **2019**, *253*, 383−391.
(48) Guo, M.; Liang, M.; Jiao, Y.; Tan, Y.; Yu, J.; Luo, D. Effect of aging and rejuvenation on adhesion properties of modified asphalt binder based on AFM. *J. Microsc.* **2021**, *284* (3), 244−255.
(49) Wang, T.; Deng, Z.; Hu, H.; Tian, F.; Ding, R.; Zhang, T.; Ma, Z.; Hou, S.; Li, X.; Dai, R.; Hong, X. Pore structure and fractal characteristics of transitional shales with different lithofacies from the eastern margin of the Ordos Basin. *Energy Science & Engineering* **2023**, *11* (11), 3979−4000, DOI: 10.1002/ese3.1580.
(50) Yao, J.; Liu, L.; Yang, Y.; Sun, H.; Zhang, L. Characterizing multi-scale shale pore structure based on multi-experimental imaging and machine learning. *Nat. Gas Ind. B* **2023**, *10* (4), 361−371, DOI: 10.1016/j.ngib.2023.07.005.
(51) Wei, J.; Zhou, X.; Shamil, S.; Yuri, K.; Yang, E.; Yang, Y.; Wang, A. Lithofacies influence characteristics on typical shale pore structure. *Energy* **2023**, *282*, No. 128728, DOI: 10.1016/j.energy.2023.128728.
(52) Siddiqui, M. A. Q.; Ali, S.; Fei, H.; Roshan, H. Current understanding of shale wettability: A review on contact angle measurements. *Earth-Sci. Rev.* **2018**, *181*, 1−11, DOI: 10.1016/j.earscirev.2018.04.002.

https://doi.org/10.1021/acsomega.4c03682
ACS Omega 2024, 9, 30859−30872